Project Title:

Computational Studies of Muon Locations, Electronic Structures and Electron Transport in High-T$_c$ Superconductor, Organic, Organometallic and Biological Systems.

Name:

◯Shukri Sulaiman (1,2), Isao Watanabe (2), Dita Puspita Sari (2,3), Muhammad Redo Ramadhan (2,4), Irwan Ramli (2,5), Wan Nurfadhilah Zaharim (1,2), Peter Greimel (2)

Laboratory at RIKEN:
(1) Universiti Sains Malaysia, Malaysia
(2) RIKEN, Nishina Center, Japan
(3) Shibaura Institute of Technology, Japan
(4) Universitas Indonesia, Indonesia
(5) Hokkaido University, Japan

1. Background and purpose of the project, relationship of the project with other projects

One of the methods that able to provide information at such microscopic properties due to high sensitivity to local magnetic and electronic environments is muon spin rotation/ relaxation/ resonance (μSR) spectroscopy. The understanding of various events such as magnetism, hyperfine interactions, and electron transport can be gained. Positively charged anti-muon, μ+ is commonly used by μSR spectroscopy as a dilute magnetic probe. μSR experiments give a measure of the microscopic field distribution at the interstitial sites where the muon stops inside the sample. Hence, the muon stopping sites is definitely important to determine electronic properties, for example, long-range magnetic ordering or localized magnetic moments.

However, μSR spectroscopy has a limitation on the determination of possible muon location. Therefore, Density Functional Theory (DFT) approach as a valuable strategy to assist μSR experiments interpretation can be used to tackle the limitations. In addition, the information on the muon stopping sites between microscopic theory and μSR data can ultimately be compared. Thus, a better understanding of the electronic structures of both pure and muoniated systems of each target materials can be accomplished.

There are six different target materials that have been studied by each user in this project. The background study and characteristic interests of each target materials are elucidated separately as below:

i. Gold nanoclusters, [Au$_{25}$(SR)$_{18}$] and [Au$_{25}$(SeR)$_{18}$]^0 with R=hexyl and ethylbenzene

Gold Nanoclusters have recently attracted significant research interest due to their fundamental physics as well as practical applications in the nanocluster technology. Metal nanoclusters refer to nano-sized Mn clusters with a diameter of less than 2 nm. What makes them different than that of the nanoparticles or even their bulk metals are because these nanoclusters display interesting optical properties such as intense photoluminescence. These properties arise from discrete electronic energy level transitions, which are available only in such extremely small particles. Due to this reason, nanoclusters are considered to be molecular in nature, behaving very different from

other forms of metals.

However, the magnetism of these materials is still unclear as discussed by Agrachev et al. Contradictory results of various experimental and theoretical investigations could be due to different ligands that cap the gold nanoclusters. Dehn et al. have observed a significant muon spin relaxation in butanethiol-capped gold nanoparticles, indicating the presence of a broad range of internal magnetic fields at the muon stopping site, which is consistent with a spatially inhomogeneous distribution of magnetic moments. This result, on the other hand, is contrary to the finding of Goikolea, where no coherent oscillations were observed from the internal field.

One of the fundamental limitations in μSR measurements is that one does not know the muon stopping sites, where the exact location of muons trapped in the sample. The pivotal point, though not granted as a priori, is the complete information of local muon couplings with its surroundings. The knowledge of the muon trapping sites, as well as hyperfine coupling constant (HFCC) are of the essence for this information to be retrieved.

In this work, we discuss the electronic structure as well as the magnetic origin and behavior of thiolate- and selenolate-gold nanoclusters. Here, we provide computational data that are probed by the muon technique within the DFT framework to validate with available experimental data, in which the possible muon stopping sites and the associated hyperfine interaction are our primary focus.
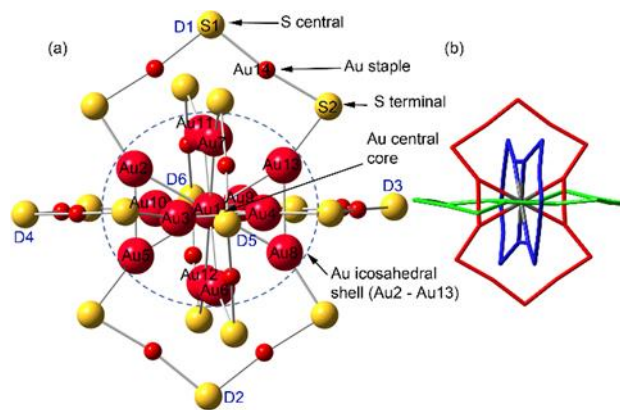
Figure 1. (a) Structure of $[Au_{25}(SR)_{18}]^0$ nanocluster modelled in the current study. The labels are used to facilitate the discussion (legend: red = Au; yellow = S). (b) Structure of three interlocked Au_8S_6 rings.

ii.   High-Tc superconducting oxides
a. $YBa_2Cu_3O_6$

$YBa_2Cu_3O_6$ (YBCO) is a typical strongly correlated system. It shows long-range antiferromagnetic (AF) ordering which is suppressed by oxygen doping ($YBa_2Cu_3O_{6+x}$) and superconductivity appear at x ~ 0.4. The detailed study of long-range AF is one key to understand how the superconductivity in this system appears. The μSR has great contribution to reveal the magnetic properties of this system. The unknown position of the implanted muon in this system prevents us to get a deeper understanding.

We approach this problem by using DFT calculation. Since YBCO is strong correlation system, we need to include Hubbard parameter, U. The U has play an important role to localize electron and establish spin. We have successfully determined three different muon-site in YBCO, which consistent with our high statistic μSR experimental data.

The internal field at each muon site can be directly extracted from the experimental data. Thus, we need to validate those internal fields by calculating the internal fields at each muon site that estimate from DFT calculation. The internal field calculations need to take in to account the zero-point vibration energy

of muon, the muon's perturbation of the system and the effect of the U value.

b. $La_{2-x}Sr_xCuO_4$

μSR method is a powerful tool to investigate the electronic state of Cu-based high-T_C superconducting oxides. To reveal muon positions inside La_2CuO_4 (LCO) gives us useful information to achieve more profound understandings of the electronic states on its magnetically ordered state. However, any unified method to investigate muon positions have not yet been firmly established. For this reason, the μSR results achieved on LCO in the early stage of high-T_C history have not yet been fully explained. We are approaching this issue by using the density functional theory (DFT) calculation technique with the additional Hubbard parameter (U) to obtain the accurate position of the implanted muon as observed in the μSR experiments.

In the current computational project, which is the final stage of the studies on the La_2CuO_4 system, we extend our calculation by varying U-values to obtain the optimized values of the Hubbard parameter. Interestingly, past studies show that there are still discrepancies of the exact U-value in past studies. In this case, not only that we obtain the accurate muon position, we also optimize the Hubbard parameter, U, which is known as one of the most important aspects that govern both magnetism and superconductivity.

iii. Organic magnets, λ-$(STF)_2FeCl_4$ and relative compounds

Band structure calculation without and with including m^+ in l-$(BETS)_2GaCl_4$. The organic superconductor l-$(BETS)_2GaCl_4$ is low-dimensional layered system offering a unique opportunity to investigate new superconducting (SC) gap states with the low Fermi surface (FS) symmetry. From our m^+SR experiment, we found that the gap structure has an unusual symmetry containing both characters of s- and d-wave symmetry in one single FS. The m^+SR experiment was done in the vortex state of this type-II superconductor. The m^+ is typically bounded to the negative charge sites, which can affect the measurement of the local vortex field especially when magnetism presents. In order to support the detail information on where the muon sites are and how the electronic structure change after injecting m^+ to the system, we carried DFT calculation. For analyzing the bands near Fermi level, we constructed Maximally localized Wannier orbital in the BETS molecules and dimers.

iv. Single and double strand 12mer synthetic DNA oligomers

Electron transport occurs in many important biological processes such as storage and consumption of energy, enzyme response, and DNA UV damage repair. μSR is an experimental technique that can be used to study electron transport phenomena in DNA at the microscopic level. The changes in the electron transport properties due to damages in DNA can be probed by using muon hyperfine interactions, which are very sensitive to the changes in the electronic structure surrounding the muonium (Mu) trapping sites. To systematically study the effect of damages on DNA to the behavior of electrons, it is, therefore, crucial to develop baseline data using DNA systems with known DNA sequences.

In the previous project, the muonium hyperfine interactions at all possible muonium trapping sites in the four nucleobases and four nucleotides were investigated. The results show that the presence of a methyl group or a sugar phosphate group to the nucleic acid bases has a direct effect on the electronic structure of the system. In FY2020, the distortion test in the geometry of guanine nucleobase when muonium is added to the possible trapping sites was conducted. An analysis on the optimized muoniated

systems structure was done to investigate whether the presence of muonium caused the guanine base ring to deviate from the planar shape. In real, DNA consists of two polynucleotide chains twisted around each other in the form of a double helix.

Each nucleotide units consist of nitrogenous bases and sugar phosphate backbone. The existence of sugar phosphate backbone and neighbouring bases can give an effect to the electronic structure of the system. Accordingly, this calculation was extend using a bigger cluster size with more bases so that the effect of neighbouring bases could be included. 12mer single strand DNA with homogeneous nitrogenous bases was chosen as a model of this study.

2．Specific usage status of the system and calculation method

Gaussian16 and Vienna Ab initio Simulation Package (VASP) software are two main ab initio quantum mechanical programs have been utilized in this group. The Gaussian program package is more suitable for the electronic structure studies of molecular systems because it employs the linear combination of atomic orbital molecular orbital (LCAO-MO) technique. The VASP software, on the other hand, which has been used in the band theory calculations for solid systems as it employs pseudopotentials or the projector-augmented wave method and a plane wave basis set. In addition, the ADF software has also been used in our computational work to provide better results on the hyperfine coupling constant (HFCC). NAMD software is used for molecular dynamics simulation and it is noted for its parallel efficiency that is often used to stimulate large system. Next, NBO for Gaussian that is based on a method for optimally transforming wave function into localized form is also used in this project. MATLAB is a high-performance language for technical computing

that integrates computation, visualization, and programming in an easy to use environment. Wannier90 also used in this project. It is an open source code for generating maximally localized Wannier functions and using them to compute advanced electronic materials with high efficiency and accuracy. For FY 2020 project, there is a total of six users have been approved for the core hours. The BWMPC resource unit is 38% of usage. It is proven that the HOKUSAI Great Wave supercomputer facility is crucial and extremely useful for our group research, particularly for the large-scale calculations due to the results obtained from the calculations by using all the resource units.

3．Result

In section 1, a considerable amount of computational effort has been done in FY2020 on the different systems is described. The data from the computational studies is collected to assist the interpretation of µSR experiments. The results for each subproject are reported separately and are as follows:

i. Gold nanoclusters, $[Au_{25}(SR)_{18}]$ and $[Au_{25}(SeR)_{18}]^0$ with R=hexyl and ethylbenzene

DFT studies of the electronic and magnetic structures in these gold nanocluster systems have been performed using the Gaussian 16 software package. Figure 2 shows the spin density distribution in $(Au_{25}SR_{18})^0$ and $(Au_{25}SeR_{18})^0$ nanoclusters. The spin densities in both systems appear to be distributed vertically along the Au_8S_6 plane but slightly inclined in different directions. Also, the surface plots of selenolate system as indicated in Figure 2(b) demonstrate a much more localized spin density distribution, centered in the vicinity of the central core (AU1).
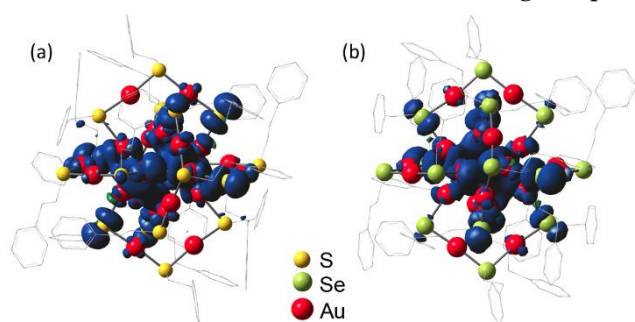
Figure 2. Isosurface plots showing spin density distribution of the $(Au_{25}SR_{18})^0$ and $(Au_{25}SeR_{18})^0$ nanoclusters presented in Au_8S_6/ Au_8Se_6 plane at isovalue of 0.004 e^-/au^3.

Figure 3(a) and Figure 3(b) show the isosurface plots of charge densities for thiolate- and selenolate-gold nanoclusters, indicating the distribution of partial charge densities throughout the systems. a significant difference exists in the charge distribution at Au13 core atoms and the outer Au12 atoms in the staple motifs. The charges on Au1 atom are -1.44 and -1.46 for the thiolated and selenolated systems, respectively. The other Au atoms in the icosehedron are relatively neutral.
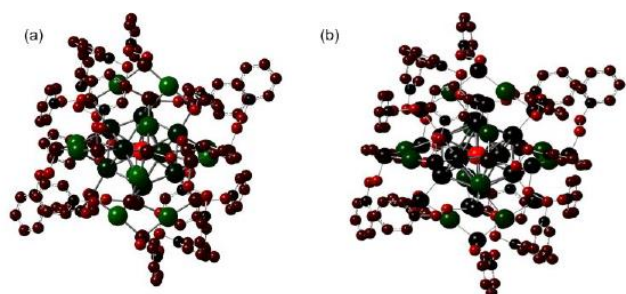
Figure 3. Charge density distribution of the (a) $(Au_{25}SR_{18})^0$ and (b) $(Au_{25}SeR_{18})^0$ nanoclusters using Natural Bond Orbital (NBO) population analysis. The color range was set to +1.00 to –1.00.

Figure 4(a) and Figure 5(b) show the MEP surface plots for the $(Au_{25}SR_{18})^0$ and $(Au_{25}SeR_{18})^0$ nanoclusters. Molecular electrostatic potential (MEP) map can be helpful to visually analyze the negatively and positively charged region of a molecule. In this study, MEP was utilized as an initial prediction tool to determine possible muon

stopping sites in both nanocluster systems. As can be seen in the figures for both systems, the Au13 inner core regions are filled with red, an indication of favorable sites for electrophilic attack. Additionally, there are also electron-rich spots in the coordinating ligands around the phenyl groups. Hence, for further muon site investigation, a total of 16 possible muon stopping sites comprising of 14 sites near the Au atoms and two other sites near the sulfur/selenium atoms were considered.
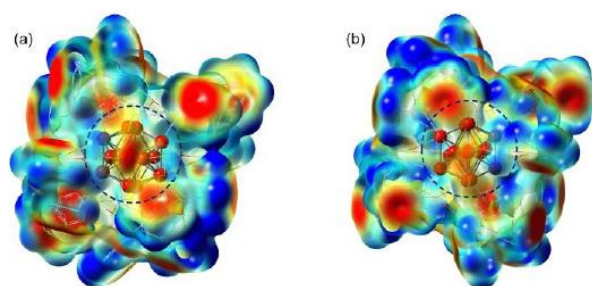
Figure 4. Molecular electrostatic potential map generated from the calculated total electron density of (a) $(Au25SR18)0$ and (b) $(Au25SeR18)0$ nanoclusters. Both maps are displayed as viewed into the Au8S6/Au8Se6 planes.

Out of the 16 possible muon sites investigated in this work, MAu11 is the site that has the lowest energy in the $(Au_{25}SR_{18})^0$ nanocluster. A muon which was initially placed at a distance of 1.640 Å from Au11 has move farther away with μ–Au11 distance being 1.757 Å after geometry optimization procedure. The position of muon and the optimized geometry of surrounding atoms are shown in Figure 5(a) and Figure 5(b). Figure 5(c) displays the inter atomic distances of the Au atoms before the introduction of a muon into the nanocluster. The calculated muon isotropic Fermi contact coupling constant *Aiso* at the MAu11 is -12.10 MHz, an indication of spin polarization effect, while the anisotropic contribution B_{aniso} is 6.44 MHz.
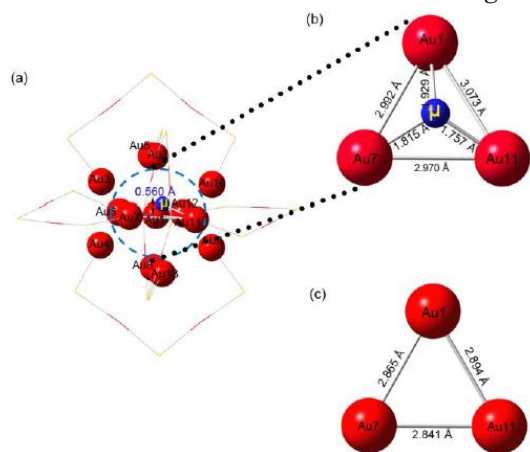
Figure 5. (a) The lowest energy muon site in $(Au_{25}SR_{18})^0$, MAu11. (b) Magnified picture of the corresponding site, showing the bond distance between μ and Au11 as well as between μ and other neighboring atoms, Au1 and Au7. (c) Au1, Au11 and Au7 interatomic distances before the introduction of a muon into the host system.

The ordering of muon sites' stability based on the relative energy for the $(Au25SeR_{18})0$ nanocluster is different than that for the $(Au25SR_{18})0$. The lowest energy muon site in the $(Au_{25}SeR_{18})^0$ nanocluster is MAu6. The Fermi contact coupling constant at the MAu6 site is only 2.85 MHz, and the sign, which is positive, is opposite to the case in the $(Au_{25}SR_{18})^0$ nanocluster. The anisotropic component B_{aniso} is 7.12 MHz, exactly the same to the one in the $(Au_{25}SR_{18})^0$ system.
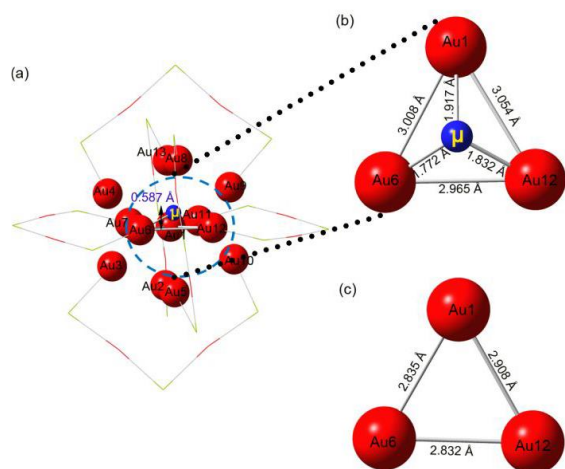
Figure 6. (a) The lowest energy muon site in $(Au_{25}SeR_{18})^0$, MAu6. (b) Magnified picture of the corresponding site, showing the bond distance between μ and Au6 as well as between μ and other

neighboring atoms, Au1 and Au12. (c) Au1, Au6 and Au12 interatomic distances before the introduction of a muon into the host system.

ii. High-Tc superconducting oxides

a. $YBa_2Cu_3O_6$

We have successfully determined three different muon sites in this system as shown in Figure 7. The internal field calculations showed the important role of zero-point vibration motion of muon, covalency effect, which caused the expansion of spin density from Cu to the planar oxygen. On the other hand, the U value is the main parameter that directly corresponds to the spin density. We optimized U value which gave the lowest difference internal field between experimental and calculation results, as shown in the Figure 8.
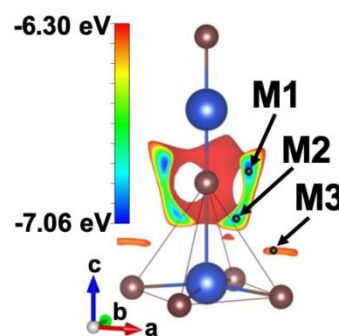
Figure 7. The muon position in the YBCO
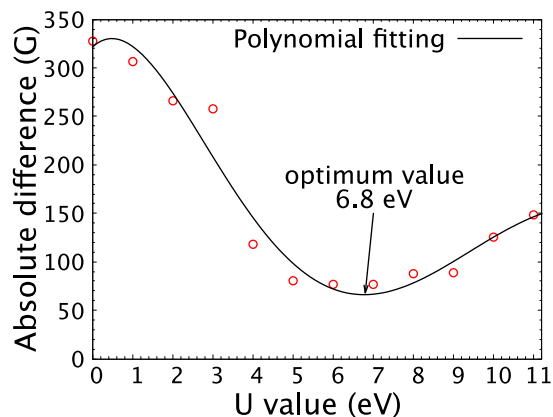
Figure 8. The absolute difference of internal fields between experimental and calculation results which fitting by polynomial function. We determined the best value of U for YBCO is 6.8 eV

b. La$_{2-x}$Sr$_x$CuO$_4$

We have reported previously that by utilizing the distributed-spin model and also zero-point vibration motion for each muon position will increases the accuracy of internal field results compared to the common point-spin model. We also confirmed the existences of three muon position inside La$_2$CuO$_4$ system ($x = 0$) that were labelled as M1, M2, and M3 following the results of electrostatic potential map that was calculated by using DFT technique. We extend this calculation, by considering the variation of U-values ranging from $2 - 8$ eV. We observed that all muon positions were not strongly affected by U-variation. The distance between the muon position with U = 2 eV and the muon position with U = 8 eV was calculated to be less than 0.06 Å. Table 1 summarizes the fractional coordinates for M1 position on La$_2$CuO$_4$

Table 1: Fractional coordinates of M1 for U = $2 - 8$ eV (only 4 U-values were shown for clarity)

U	M1 fractional coordinate		
(eV)	a-axis	b-axis	c-axis
2	0.3774	0.6188	0.4380
4	0.3777	0.6180	0.4378
6	0.3779	0.6169	0.4372
8	0.3783	0.6152	0.4365

With the additional information on the asymmetry parameter from μSR experiment, we observed that the ratio between each muon position is 10.6:3:1. With those information, we calculated the absolute difference between μSR experimental data and DFT results, and fit the data using the Gaussian function. We obtained that the best U-value for the La$_2$CuO$_4$ system is 4.94(2) eV as described in Figure 9. This U-value produces a stable antiferromagnetic insulating system with 0.52 μ$_B$ and band gap 1.2 eV

which corresponds well with the known experimental results. We have submitted those results to PRL. The current situation is "reviewed now".
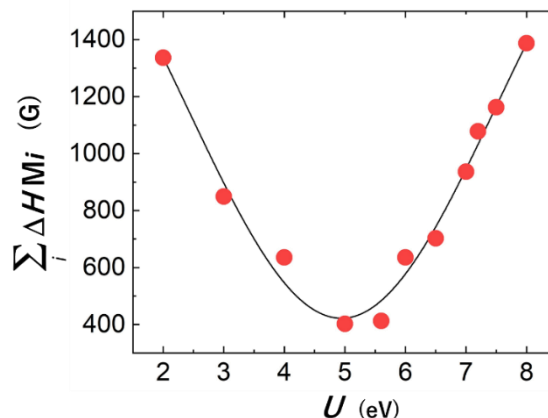
Figure 9. Optimization of U-values in terms of absolute difference between μSR and DFT results.

iii. Organic magnets, λ-(STF)$_2$FeCl$_4$ and relative compounds

Figure 10(a) show the band structure of l-(BETS)$_2$GaCl$_4$. The 4 bands near the Fermi level represent the four BETS molecule in unit cell. The highest occupied molecular orbital (HOMO) is ¾ filled in this case (molecule model). However, the dimerization makes the system can be treated as 1/2-filled (dimer model). Then, two upper band represent two dimers in unit cell. The molecule and dimer model of the Wannier band can well reproduce the DFT bands, shown in Fig. 10(a). From the minimum electronic potential calculation, we found that the muon site is at in between the edge of BETS molecule and the GaCl$_4$ the coordinate x = 0.675, y = 0.605, z = 0.915 in regard of the unit cell, shown in Figure 8(b). From here, we can see that the muon site is quite at the center of the unit cell, not only concentrated or bounded in the negative charge.

Indeed, we loss some amount of Asymmetry due to muonium. But the m$^+$ still be able to sense the local vortex field since it is also close to the Hydrogen

molecule (the edge of BETS molecules). Furthermore, we injected one m^+ in the unit cell. The band structure does barely change after injecting m^+ as shown in Fig. 10(a). Note that the m^+ injection in the actual system should be much more dilute. This result support that the electronic structure in the metallic state did not so much change due to m^+ and so did not the SC vortex state.
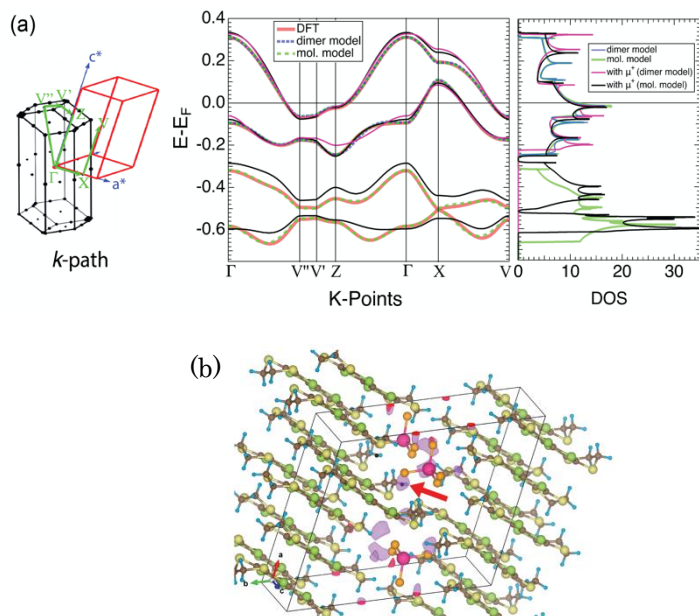
Figure 10 (a) Result of electronic minimum potential calculation by DFT. (b) Red arrow indicates the muon site in the crystal where the potential is minimum. The purple area in (a) is the isosurface of 37.85 eV.

iv. Single and double strand 12mer synthetic DNA oligomers

In principle, the addition of muonium will alter the atomic charge of the C8 atom. The atomic charge on C8 atoms in the different Mu-12mer single strand DNA oligomer complexes varies from -0.064 to -0.051. The results show that all C8 atoms have a slightly negative atomic charge value. The addition of muonium to the C8 atoms caused the atomic charges on the C8 atoms to become more negatively compared to the pure system with differences of

about 14% to 19%. The C8 and B9 complex has the highest negative charge, with a corresponding value of -0.0064. the atomic charge on muonium in different complexes varies from 0.121 to 0.133. muonium in B12 complex has the highest positive charge, which is 0.133.

The highest occupied molecular orbital (HOMO) and lowest unoccupied molecular orbital (LUMO) molecular orbital energies were obtained by using the B3LYP/6-311++G(d,p) level of theory. The LUMO energy level values for all possible muonium trapping sites are quite similar and are in the range of -2.039 eV to -2.200 eV. The addition of muonium to the atom in guanine base ring does not lead to a notable change to the LUMO energies. This observation is similar with the small systems. However, the situation is different in the case of HOMO energy. There is a considerable fluctuation in the value of the HOMO energy.

The calculated HOMO energy in the range of -4.175 eV to -5.364 eV, a variation about 1.2 eV which is very significant. The HOMO energy of the muoniated systems is higher than the pure system (-5.365 eV). The corresponding HOMO-LUMO energy gap values are in the range of 2.114 eV to 3.248 eV. The HOMO-LUMO energy gap, followed by B5 and B3. It is clear that the addition muonium to different guanine bases in the same system results in a significant effect on the HOMO-LUMO energy gap.

Moreover, for this FY we have successfully obtain the optimized structure of the other single strand DNA which is 12mer single strand cytosine and adenine DNA oligomer. We are now analyzing the data that we have obtained.

4．Conclusion

i. Gold nanoclusters, $[Au_{25}(SR)_{18}]$ and $[Au_{25}(SeR)_{18}]^0$

with R=hexyl and ethylbenzene

Our present work results show that ligand effects are quite significant in affecting the position of muon in Au nanocluster. In $(Au_{25}SR_{18})^0$, the most stable muon site is MAu11 while in $(Au_{25}SeR_{18})^0$, MAu5 is the one with the lowest energy. In our previous work using the hexanethiol ligands, $S(CH_2)_5CH_3$, the most stable muon site was found to be MAu10. In terms of hyperfine interaction, the anisotropic component does not change much at different muon sites. On the other hand, the isotropic component was quite sensitive to different ligands, varying in magnitudes and signs. It was found that, the hyperfine coupling constant for the most stable sites in the $(Au_{25}SR_{18})^0$ and $(Au_{25}SR_{18})^0$ are -5.66 MHz and 9.57 MHz, respectively.

ii.   High-Tc superconducting oxides
a. $YBa_2Cu_3O_6$

We have successfully estimated the muon site in YBCO and calculated the internal fields at the muon site as function of U. We determined the U value for YBCO to be 6.8 eV by directly comparing the experimental and calculation results

b. $La_{2-x}Sr_xCuO_4$

DFT+U with the exchange correlation function of GGA PW91 was successfully employed to obtain accurate muon position from the parent compound of high-T_C superconducting cuprate, La_2CuO_4.To elucidate the relations between Hubbard parameter (U) with the calculated parameters, we varied the U-values from 2 – 8 eV and observed that the muon position did not change with the variation of Hubbard parameter. By utilizing distributed-spin model and the consideration of quantum behavior of the muon, we observe that the best U-values for the

La_2CuO_4 is 4.94(5) eV precisely, providing accurate information of the electronic states in La_2CuO_4 and also proposing a novel way to utilize μSR experiment on many strongly correlated systems.

iii. Organic magnets, λ-(STF)2FeCl4 and relative compounds

DFT calculation has been carried out for estimating m^+ stopping site and band structure before and after injecting m^+ at the stopping site in the organic superconductor l-(BETS)₂GaCl₄. From the minimum electronic potential calculation, we found that the muon site is at in between the edge of BETS molecule and the $GaCl_4$ the coordinate x = 0.675, y = 0.605, z = 0.915 in regard of the unit cell. The band structure does barely change after injecting m^+. Assuming that the m^+ injection in the actual system should be much more dilute, the electronic structure in the metallic state did not so much change due to m^+ and so did not the SC vortex state.

iv. Single and double strand 12mer synthetic DNA oligomers

The optimized structure of 12mer single strand guanine oligomer have been obtained. Based on the total energy, DFT method performed better than the semi-empirical method in obtaining the predicted optimized atomic arrangement of the system. The optimized structures from the DFT calculation maintain a planar form. The calculated HOMO-LUMO gap is 3.313 eV. The amount of reduction in the HOMO-LUMO gap is close to 2 eV. Consequently, the optimized DFT structure was used to continue the study involve Mu.

5．   Schedule and prospect for the future

On the basis of our achievements in 2020, we plan to

perform more complex calculations on our target systems and try to gain the following goals. We expect to continue and perform more complex calculations on our target systems. Therefore, more time is required, and it is of great importance for us to pursue our usage in HOKUSAI GreatWave supercomputer for FY2021.

i.　High-Tc superconducting oxides
a. $YBa_2Cu_3O_6$

The number of muons that stop in each position is different for each muon sites. We will try to include the initial asymmetry for each muon precession component in the determination of precise determination of the U value.

b.　$La_{2-x}Sr_xCuO_4$

Due to the size of the supercell calculation (~1000 atoms with non-collinear spin) and the new extension of the calculation in the form of U-variation, we cannot complete the calculation on the doped system on this project. However, with the more refined U-values on La_2CuO_4, we can limit the amount of calculations that need to be done in the case of doped system with the Sr atom or Ba atom. This will be the main focus and be explained in detail on the next HOKUSAI project.

ii. Organic magnets, λ-$(STF)_2FeCl_4$ and relative compounds

For the next plan, we would like to extend the calculation to the other sister compounds of the l-$(D)_2GaCl_4$ family with a different cation such as STF, ET, or BEST. This family is recently attracting attention since it seemed to be an unconventional strongly correlated system with the superconducting

(SC) state is near by the Antiferromagnetic (AF) state with the Mott transition. Although, in this system there is no such p-d interaction like it has been in the l-$(D)_2FeCl_4$ family. The calculation will focus on the m$^+$ stopping site, band structure, FS shape, and transfer integral lattice. We also plan to chase another organic superconductor which has a different type of stacking molecule in the conducting plane, e. g. k-type superconductor whose FS symmetry is higher than that of l-type family.
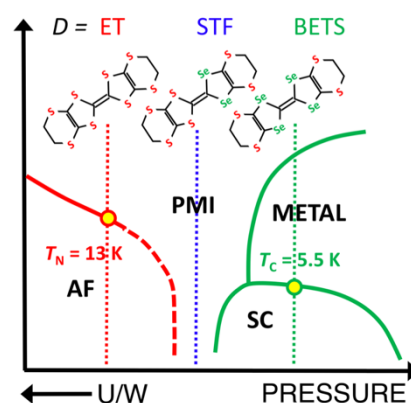
Figure 11. The P-T schematic phase diagram of the l-$(D)_2GaCl_4$ family determined by the magnetic susceptibility, resistivity and NMR, and m$^+$SR experiments.

iii. Single strand synthetic DNA model molecules

The electronic structure of muoniated 12mer single strand adenine and cytosine oligomer. Details information on the muoniated radicals of 12mer single strand adenine and cytosine oligomers are needed. Thus, in the next fiscal year, we would like to obtain the electronic structure of muoniated 12mer single strand adenine and cytosine oligomer. After completing the analyzation on these two oligomer, we will continue the optimization calculation work on 12mer single strand thymine oligomer.

Fiscal Year 2020 List of Publications Resulting from the Use of the supercomputer

[Paper accepted by a journal]

1. Ahmad, S. N., Zaharim, W. N., Sulaiman, S., Hasan Baseri, D. F., Mohd Rosli, N. A., Ang, L. S., ... & Watanabe, I. (2020). Density Functional Theory Studies of the Electronic Structure and Muon Hyperfine Interaction in $[Au_{25}(SR)_{18}]^0$ and $[Au_{25}(SeR)_{18}]^0$ Nanoclusters. *ACS omega.* (published)(WOS Indexed)

2. Zaharim, W. N., Rozak, H., Sulaiman, S., Ahmad, S. N., Hasan Baseri, D. F., Mohd Tajudin, S. S., Ang, L. S., & Watanabe, I. Density Functional Theory Investigation of Hyperfine Interaction in DNA Nucleobase and Nucleotide Muoniated Radicals. *J. Phys. Soc. Jpn.* (accepted)(WOS Indexed)

[Conference Proceedings]

1. Ramadhan, M.R., Ramli, I., Sari, D.P., Kurniawan, B., Manaf, A., Mohamed-Ibrahim, M.I., Sulaiman, S., Watanabe, I. Spin alignment Studies on the Muon-Site Determination in La_2CuO_4. *Key Engineerring Materials Journal.* 860, 154. (SCOPUS Indexed)

2. Zaharim, W. N., Sulaiman, S., Mohd Tajudin, S. S., Abu Bakar, S. N., Ismail, N. E., Rozak, H., & Watanabe, I. (2020). Basis Set Effects in Density Functional Theory Calculation of Muoniated Cytosine Nucleobase. In *Key Engineering Materials* (Vol. 860, pp. 282-287). Trans Tech Publications Ltd. (SCOPUS Indexed)

[Oral presentation]

1. Zaharim, W. N., Sulaiman, S., Watanabe, I. (September, 2020). Computational Studies on Muonium Trapping Sites in Guanine. Oral presentation at *Muon Site Calculation Meeting 2020.* Harwell, United Kingdom. (ONLINE)

2. Sulaiman, S. (July, 2020). DFT Studies on the Electronic Strycture of DNA and Gold Nanocluster. *Keynote Speaker at International Conference on Functional Materials Science 2020.* Universitas Indonesia, Indonesia. (ONLINE)

3. Sari, D. P. (July, 2020). Understanding Electronic Structure Calculation on Organic Molecular Based Superconductor λ-$(BETS)_2GaCl_4$ by using VASP. *Keynote Speaker at The Webinar Series "Introduction on computational Material Science"* Institut Teknologi Sepuluh Nopember, Surabaya, Indonesia. (ONLINE)

4. Sari, D. P. (November, 2020). Distorted Superconducting Nodal Line on Single Fermi Surface in Organic Superconductor λ-$(BETS)_2GaCl_4$. *Invited speaker at The 5th International Symposium of Quantum Science "Chirality in Materials Science: Current Status and Future Prospects"* Ibaraki University, Ibaraki, Japan. (ONLINE)

[Poster presentations]